Mon. Not. R. Astron. Soc. **364,** 665–673 (2005) doi:10.1111/j.1365-2966.2005.09601.x

Cusps in cold dark matter haloes

Jürg Diemand,[1,3]★ Marcel Zemp,[1,2] Ben Moore,[1] Joachim Stadel[1] and Marcella Carollo[2]

[1]*Institute for Theoretical Physics, University of Zürich, Winterthurerstrasse 190, CH-8057 Zürich, Switzerland*
[2]*Institute of Astronomy, ETH Zürich, ETH Hönggerberg HPF D6, CH-8093 Zürich, Switzerland*
[3]*Department of Astronomy and Astrophysics, University of California, 1156 High Street, Santa Cruz, CA 95064, USA*

Accepted 2005 September 6. Received 2005 September 3; in original form 2005 April 11

ABSTRACT

We resolve the inner region of a massive cluster forming in a cosmological Λ cold dark matter (CDM) simulation with a mass resolution of 2×10^6 $M_\odot$ and before $z = 4.4$ even 3×10^5 $M_\odot$. This is a billion times less than the cluster's final virial mass and a substantial increase over current ΛCDM simulations. We achieve this resolution using a new multimass refinement procedure and are now able to probe a dark matter halo density profile down to 0.1 per cent of the virial radius. The inner density profile of this cluster halo is well fitted by a power law $\rho \propto r^{-\gamma}$ down to the smallest resolved scale. An inner region with roughly constant logarithmic slope is now resolved, which suggests that cuspy profiles describe the inner profile better than recently proposed profiles with a core. The cluster studied here is one out of a sample of six high-resolution cluster simulations, and its inner slope of about $\gamma = 1.2$ lies close to the sample average.

Key words: methods: *N*-body simulations – methods: numerical – galaxies: clusters: general – galaxies: haloes – dark matter.

1 INTRODUCTION

Recently, a great deal of effort has gone into high-resolution simulations which have revealed density profiles of cold dark matter (CDM) haloes down to scales well below one per cent of the virial radius (Diemand et al. 2004b, hereafter DMS04; Fukushige, Kawai & Makino 2004; Navarro et al. 2004; Tasitsiomi et al. 2004; Reed et al. 2005). However, the form of profile below ∼0.5 per cent of the virial radius remained unclear and there was no clear evidence for a cusp in the centre, i.e. no significant inner region with a constant logarithmic slope. Galaxy cluster haloes would be the ideal systems to resolve cusps numerically because of their low concentration. In a galaxy or dwarf halo, the inner power law is much harder to resolve because it lies at a smaller radius relative to the size of the system.

The existence of a core or a cusp in the centre of CDM haloes has important observational consequences and is the crucial point in many tests of the CDM theory. Comparisons of dark matter simulations to rotation curves of low surface brightness (LSB) galaxies seem to favour constant density cores for most observed systems (e.g. Flores & Primack 1994; Moore 1994; Salucci & Burkert 2000; deBlock et al. 2001; see, however van den Bosch & Swaters 2001; Swaters et al. 2003; Simon et al. 2005). However, these comparisons still depend to some extent on extrapolations of the simulated profiles toward the centre: Stoehr (2004) extrapolate to a constant density core and claim that the discrepancy to LSB galaxy rotation curves is much smaller than previously believed.

The strength of the γ-ray signal from dark matter annihilation depends on the square of the dark matter density and the calculated flux values spread over several orders of magnitude, depending on how one extrapolates the density profiles from the known, resolved regions down into the centres of the galactic halo and its subhaloes (Calcaneo-Roldan & Moore 2000; Stoehr et al. 2002; Prada et al. 2004; Bertone & Merrit 2005). Small, very abundant, Earth to solar mass subhaloes could be very luminous in γ-rays if they are cuspy (Diemand, Moore & Stadel 2005).

The highest resolutions in cosmological simulations are reached with the widely used refinement procedure (e.g. Bertschinger 2001). First, one runs a simulation at uniform, low resolution and selects haloes for resimulation. Then, one generates a new set of initial conditions using the same large-scale fluctuations and higher resolution and additional small-scale fluctuations in the selected region. With this technique Navarro, Frenk & White (1996) were able to resolve many haloes with a few ten thousand particles and to infer their average density profile, which asymptotes to an $\rho(r) \propto r^{-1}$ cusp. Other authors used fitting functions with steeper (−1.5) cusps (Fukushige & Makino 1997; Moore et al. 1998, 1999; Ghigna et al. 2000). Small-mass CDM haloes have higher concentrations due to their earlier collapse (Navarro et al. 1996) but the slopes of the inner density profiles are independent of halo mass (Moore et al. 2001; Colín et al. 2004). Open, 'standard' and lambda CDM cosmologies, i.e. models with $(\Omega_M, \Omega_\Lambda) = (0.3, 0.0), (1.0, 0.0)$ and $(0.3, 0.7)$ yield

★E-mail: diemand@physik.unizh.ch

Table 1. Parameters of the simulated cluster. At $z = 0$ the viral mass is 3.1×10^{14} $M_\odot$ and the virial radius is 1.75 Mpc. N_{HR} is the number of high-resolution particles and m_{HR} is the mass and ϵ_{HR} the force softening length of these particles. For the multimass runs we also give the masses (m_{LR}) and softenings (ϵ_{LR}) of the next heavier particle species. Softening lengths are given at $z = 0$; '[c]' indicates that a constant softening in comoving coordinates was used and '[p]' indicates that the softening was constant in physical units after $z = 9$ and constant at 10 times this value in comoving units before $z = 9$. The resolved scales are constant in physical units and give the innermost radius we expect to resolve with the given mass resolution. $N_{vir,eff}$ is the actual number of particles within the virial radius at $z = 0$ for runs D6, D9 and D12. For the multimass runs it is the number needed to reach the same resolution in the inner part by carrying out a conventional refinement of the entire system. All runs are 300-Mpc cubes with periodic boundaries; well outside the cluster-forming region the resolution is decreased (as in DMS04).

Run	z_{start}	z_{end}	ϵ_{HR} (kpc)	N_{HR}	m_{HR} ($M_\odot$)	ϵ_{LR} (kpc)	m_{LR} ($M_\odot$)	$r_{resolved}$ (kpc)	η	Time-step	$N_{vir,eff}$
D5	52.4	0	4.2[p]	4 898 500	3.0×10^8	–	–	16.2	0.25	(1)	1.0×10^6
D6	36.13	0	3.6[p]	31 922 181	1.8×10^8	–	–	13.5	0.2	(1)	1.8×10^6
DM6se	36.13	0	3.6[p]	922 968	1.8×10^8	3.6[p]	3.8×10^{10}	13.5	0.2	(1)	1.8×10^6
DM6le	36.13	0	3.6[p]	922 968	1.8×10^8	38.6[p]	3.8×10^{10}	13.5	0.2	(1)	1.8×10^6
D9	40.27	0	2.4[p]	31 922 181	5.2×10^7	–	–	9.0	0.2	(1)	6.0×10^6
DM9	40.27	0	2.4[p]	3 115 017	5.2×10^7	15[p]	1.4×10^9	9.0	0.2	(1)	6.0×10^6
D12	43.31	0	1.8[p]	14 066 458	2.2×10^7	–	–	6.8	0.2	(1)	1.4×10^7
DM25	52.4	0.8	0.84[c]	65 984 375	2.4×10^6	9[c]	3.0×10^8	3.3	0.25	(2)	1.3×10^8
DM25lt	52.4	0.8	0.84[p]	65 984 375	2.4×10^6	9[p]	3.0×10^8	3.3	0.25	(1)	1.3×10^8
DM50	59.3	4.4	0.36[c]	16 125 000	3.0×10^5	6[c]	3.75×10^7	1.7	0.25	(2)	1.0×10^9

equal inner profiles (Fukushige & Makino 2003; Fukushige et al. 2004). There is some indication that models with less small-scale power such as warm dark matter lead to shallower inner profiles (e.g. Colín, Avila-Reese & Valenzuela 2000; Reed et al. 2005). Different equation of states of the dark energy component lead to different collapse times and halo concentrations but it is not clear yet if it also affects slopes well inside of the scale radius (Macciò et al. 2004; Kuhlen et al. 2005). Most current simulations do not resolve a large enough radial range to determine both the concentration and the inner slope; at the current resolution these parameters show some degeneracy (Klypin et al. 2001).

Recently, a large sample of ΛCDM haloes resolved with a million and more particles was simulated (Springel et al. 2001; Navarro et al. 2004; Tasitsiomi et al. 2004; Gao et al. 2005; Reed et al. 2005) and the best resolved systems contain up to 25 million particles (DMS04; Fukushige et al. 2004). However, even these very large, computationally expensive simulations resolved no inner region with a constant logarithmic slope. Navarro et al. (2004), Stoehr et al. (2002) and Stoehr (2004) introduced cored profiles which seem to fit the simulation data better than the cuspy profiles proposed earlier by Navarro et al. (1996) and Moore et al. (1999). This better fit was interpreted as indication against cuspy inner profiles. However, these cored profiles have one additional parameter and therefore it is not surprising that they fit the data better. DMS04 have shown that an NFW-like profile with the inner slope as an additional free parameter fits the highest-resolution profiles just as well as cored profiles. Some theoretical arguments seem to favour cusps (e.g. Binney 2004; Hansen & Moore 2005) but make only vague predictions about the inner slopes. A recent model combines simulation results and analytical arguments to predict an inner slope of -1.27 (Ahn & Shapiro 2005). At the moment higher-resolution simulations seem to be the only way to decide the core versus cusp controversy.

Here we present simulations of one of the galaxy clusters from DMS04 with two orders of magnitude better mass resolution. Our results give strong support to cuspy inner profiles. This increase in resolution was made possible with only a moderate increase in computational cost by using a new multimass refinement technique described in Section 2. In Section 3 we present our results and in Section 4 the conclusions.

2 NUMERICAL EXPERIMENTS

Table 1 gives an overview of the simulations we present in this paper. All runs discussed in this paper model the same ΛCDM cluster labelled 'D' in DMS04. With a mass resolution corresponding to 1.3×10^8 and 1.04×10^9 particles inside the virial radius of a cluster, DM25 and DM50 are the highest-resolution ΛCDM simulation performed so far. Due to the large number of particles and the corresponding high force and time resolution, these runs take a large amount of CPU time. Fortunately, the inner profiles of CDM clusters are already in place around redshift one and evolve little between $z = 4$ and $z = 0$ (Fukushige et al. 2004; Tasitsiomi et al. 2004; Reed et al. 2005). Therefore, one does not have to run the simulations to $z = 0$ to gain insight into the inner density profile. We stop DM50 at $z = 4.4$, DM25 at $z = 0.8$ and use the medium-resolution runs D5 and D12 to quantify the low-redshift evolution of the density profile of the same cluster. Run DM25 was completed in about 2×10^5 CPU hours on the zBox supercomputer.[1] The convergence radius of run DM50 is 1.7 kpc, estimated using the $r \propto N^{-1/3}$ scaling and the measured converged scales from DMS04.

2.1 Multimass refinements

Often in cosmological N-body simulations one uses high-resolution particles only where one halo forms and heavier particles in the surroundings to account for the external tidal forces. One usually tries to defines a large enough high-resolution region to minimize or avoid mixing of different mass particles within the region of interest. One exception is Binney & Knebe (2002) who used particles of two different masses everywhere to estimate the amount of two-body relaxation in cosmological simulations. In plasma simulations, on the other hand, multimass simulations have been successfully used since the 1970s (e.g. Dawson 1983, and references therein). Here we apply this idea to increase the resolution in the core of one cluster halo in a cosmological N-body simulation.

The refinement procedure is usually applied to entire virialized systems, i.e. one marks all particles inside the virial radius of the

[1] See http://www-theorie.physik.unizh.ch/~stadel/zBox/.

selected halo and traces them back to the initial conditions. Then one refines the region that encloses the positions of the marked particles. Usually the region is further increased to prevent any mixing of low-resolution particles into the virial radius of the final system. In DMS04 all particles within 4 comoving Mpc in the initial conditions were added to the high-resolution region. This ensures that only light particles end up within the virial radius of the final cluster and it also has the advantage that haloes in the outskirts of the cluster (out to two or three virial radii) are still well resolved (Moore, Diemand & Stadel 2004). However, with this procedure only between one-fourth to one-third of all the high-resolution particles end up in the cluster.

If one is only interested in the inner regions of a halo, it is possible to use a new, more efficient way of refinement. Instead of refining the whole virialized system, we only refine the region where the inner particles come from. This allows us to reduce the size of the high-resolution region considerably, because most of particles that end up near the centre of the system start in a very small region, compared to the region which one finds by tracing back all the particles inside the virial radius. Using this technique, it is possible to reduce the computational cost of a CDM cluster simulation by at least one order of magnitude at equal force and mass resolution in the inner region. Of course, now one has different mass particles inside the final virialized structure, and therefore we must verify that significant equipartition and relaxation (Binney & Knebe 2002; Diemand et al. 2004a) are not occurring and affecting the final results. In Section 2.3 we show that the density profiles of such multimass clusters (runs DM6le and DM9) are the same as those of fully refined clusters at equal peak resolution (runs D6 and D9).

In this paper we apply the multimass refinement to the cluster 'D' from DMS04. This cluster is well relaxed and isolated at $z = 0$ and has an average density profile and inner slope close to the mean value. First, we mark all particles within one per cent of the virial radius in the final halo and trace them back to the initial conditions. Then we add all particles within one comoving Mpc of a marked particle to the set of marked particles, and finally we add all particles which lie on intersections of any two already marked particles on the unperturbed initial grid positions. After these two steps, there is region with a fairly regular triaxial boundary which contains only marked particles. The number of marked particles grows by almost a factor of 8 during these additions, but it is still more than a factor of 2 smaller than the number of particles in the final cluster and a factor of 10 smaller than the original high-resolution volume used in DMS04. The computational cost with our code and parameters is roughly proportional to the number of high-resolution particles, and therefore we gain about a factor of 10 with this reduction of the high-resolution region. Probably one can reduce the high-resolution volume further and focus even more of the computational effort into the innermost region, we plan to explore this possibility with future simulations.

2.2 Code and parameters

The simulations have been performed using PKDGRAV, written by Joachim Stadel and Thomas Quinn (Stadel 2001) using the same cosmological and numerical parameters as in DMS04 with a few changes given below and in Table 1. The cosmological parameters are $(\Omega_{\rm m}, \Omega_\Lambda, \sigma_8, h) = (0.268, 0.732, 0.7, 0.71)$. The value of $\sigma_8 = 0.9$ given in DMS04 is not correct: during the completion of this paper we found that, due to a mistake in the normalization, our initial conditions have less power than intended. This lowers the typical formation redshifts and halo concentrations slightly but does not affect the slopes of the inner density profiles.

We use the GRAFICS2 package (Bertschinger 2001) to generate the initial conditions. The particle time-step criterion $\Delta t_i < \eta\sqrt{\epsilon/a_i}$, where a_i is the acceleration of particle 'i', gives almost constant time-steps in the inner regions of a halo (see fig. 2 in DMS04), but the dynamical times decrease all the way down to the centre. Therefore, the time-step criterion was slightly modified, to make sure enough time-steps are taken also near the halo centres. Instead of

$$\Delta t_i < \eta\sqrt{\epsilon/a_i} \tag{1}$$

we now use

$$\Delta t < \min\left(\eta\sqrt{\epsilon/a_i}, \eta/4\sqrt{G\rho_i}\right), \tag{2}$$

where ρ_i is the density at the position of particle 'i', obtained by smoothing over 64 nearest neighbours. We used $\eta = 0.25$ for runs DM25 and DM50. Note that in the inner region of a CDM halo $\rho(r) \simeq 0.6\ \rho(<r)$, i.e. $0.8\sqrt{G\rho(r_i)} \simeq \sqrt{G\rho(<r_i)}$. Therefore, the condition (2) with $\eta = 0.25$ ensures that at least 12 time-steps per local dynamical time $1/\sqrt{G\rho(<r_i)}$ are taken.

The time-steps are obtained by dividing the main time-step ($t_0/200$) by a factor of 2 until condition (2) is fulfilled. In runs DM25 and DM50 the smallest particle time-steps are $t_0/51200$. According to fig. 2 in DMS04, this time-step is sufficient to resolve smaller scales than 0.1 per cent of the virial radius, i.e. less than the limit set by the mass resolution, even in run DM50.

The smaller time-steps in the inner regions of the cluster are crucial. In Fig. 1 we compare two runs which only differ in the time-step criterion. DM25lt was run with the standard criterion (1) and $\eta = 0.2$; for run DM25 we used the more stringent, computationally more expensive criterion (2) and $\eta = 0.25$. The difference in CPU time is about a factor of 2. At $z = 0.8$ the densities in run DM25lt are clearly lower out to 0.003 virial radii, which also affects part of the region we aim to resolve with this run ($r_{\rm resolved} = 0.0019 r_{\rm vir}$). Due to the high computational cost of these runs, we cannot perform a complete series of convergence test at this high resolution. However, due to the monotonic convergence behaviour of PKDGRAV for shorter

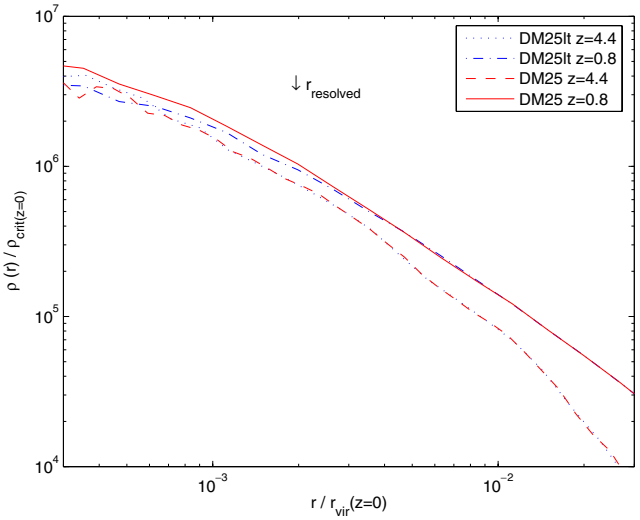

Figure 1. Density profiles in physical (not comoving) coordinates at redshifts 4.4 and 0.8. The two runs have equal mass resolution but different time-steps and softening. The arrow indicates the resolution limit set by the particle mass. The run with the larger time-steps and softening underestimates the dark matter density outside the resolution scale.

time-steps (Power et al. 2003) we are confident that DM25 is a better approximation to the true CDM density profile of this cluster.

Our time-stepping test confirms that the time resolution in DMS04 was sufficient to resolve the minimum scale of 0.3 per cent virial radii set by their mass resolution. For the purpose of this work, i.e. to resolve a region even closer to the centre, smaller time-steps are necessary. These two runs illustrate nicely how a numerical parameter or criterion that passes convergence tests performed at low or medium resolution can introduce substantial errors if employed in high-resolution runs.

2.3 Testing the multimass technique

Reducing the high-resolution region in the way described in Section 2.1 produces multimass virialized systems, i.e. haloes where particles of different mass are mixed up with each other. The inner regions are dominated by light particles and the region near the virial radius by heavier particles. However, one will find particles of both species everywhere in the final halo and one has to worry if this mixing introduces numerical effects, such as energy transfer from the outer part to the inner part (from the heavy to the light particles) due to two-body interactions. This could lead to numerical flattening of the density profile and make heavy particles sink to the centre (Binney & Knebe 2002; Diemand et al. 2004a).

To check if the multimass technique works for cosmological simulations we reran the simulations D6 and D9 from DMS04 using a reduced high-resolution region. We call these multimass runs 'DM6se', 'DM6le' and 'DM9' (see Table 1). The next heavier particles in the surrounding region are 216 times more massive in DM6se and DM6le and 27 times more massive in DM9. The heavier particles in DM6le and DM9 have larger softening to suppress discreteness effects while DM6se uses the same small softening for both species. Fig. 3 shows that the density profiles of the fully refined run D9 and the partially refined run DM9 are identical over the entire resolved range. Fig. 2 shows that the same is true for run DM6le; the larger mass ratio of 216 does not introduce any deviation form the density profile of the fully refined run.

A small softening in the heavier species (run DM6sl) does introduce errors in the final density profile (Fig. 2). The total mass profile is shallower near the resolved radius and has a high-density bump below the resolved scale. The light particles are more extended and the bump is caused by a cold, dense condensation of six heavy particles within $0.004 r_{\rm vir}$. These six heavy particles have a three-dimensional velocity dispersion of only 273 km s^{-1}, while the light particles in the same region are much hotter, $\sigma_{\rm 3D} = 926$ km s^{-1}. They are hotter than the particles in the same region in runs D6 and DM6le (both have only light particles in this inner part), and the dispersions are 722 km s^{-1} for D6 and 708 km s^{-1} for DM6le.

These tests indicate that the reduced refinement regions work well in runs D9M and DM6le and therefore we used the same refinement regions to set up the higher-resolution run DM25. In this run the heavier particles are 125 times more massive than the high-resolution particles and they have a softening of 9 kpc. For run DM50 we refined only the inner part of the most massive cluster progenitor at $z = 4.4$ in the same way as the final cluster in runs DM6le, DM6se, DM9 and DM25. In run DM50, the heavier particles are also 125 times more massive than the high-resolution particles.

Fig. 3 shows how the initially separated species of light and heavy particles mix up during the the runs DM9, DM25 and DM50. The density profiles of DM6le and DM9 do not suffer from numerical effects due to the multimass set-up. This indicates that the same is true for run DM25, which has the same refinement regions. In run DM50, the amount and location of mixing at $z = 4.4$ relative to r_{200} is very similar to the situation for DM9 at $z = 0.0$; therefore, we expect DM50 to have the same density profile as a fully refined cluster, i.e. as a cluster resolved with a billion particles.

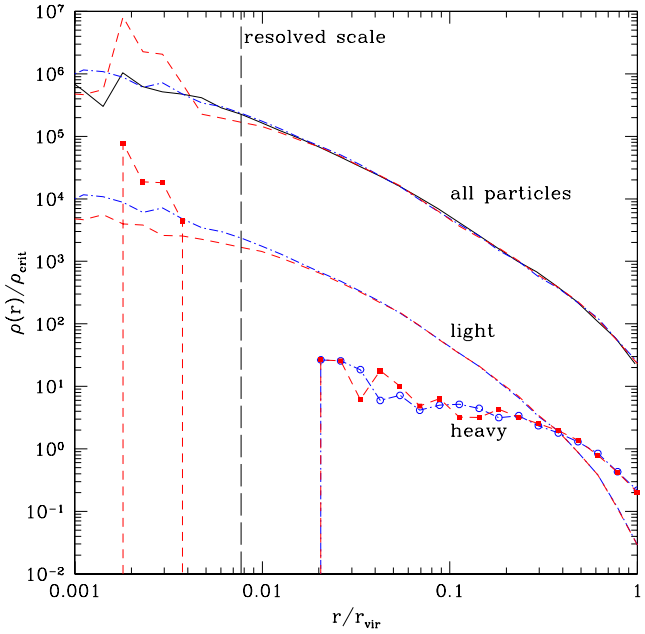

Figure 2. Tests of the multimass refinement technique. The upper three lines shows the total density profile at $z = 0$ from the fully refined run D6 (solid lines) and the multimass runs DM6se (dashed) and DM6le (dashed dotted). The lower lines (same line styles, offset by two magnitudes for clarity) show the density profiles of the two particle species, i.e. of the light ones (lines without symbols) and of the heavier ones (lines with symbols: filled squares for D6se, open circles for D6le). The vertical dashed line indicates the innermost resolved scale. In the multimass run with more softened heavier particles (D6lh) the inner profile is dominated by light particles and is identical to the fully refined run of the same cluster (D6). When the heavier particles have short softenings, some of them spiral into the centre due to dynamical friction and transfer heat to the light particles. This affects the total density profile, i.e. it is lower near the resolved scale and has a bump due to a condensation of cold, massive particles very close to the centre.

3 INNER DENSITY PROFILES

Here we try to answer the question if the inner density profiles of dark matter haloes have a constant density or a cusp $\rho(r) \propto r^{-\gamma}$. At resolutions of up to 25 million particles within the virial radius there is no evident convergence toward any constant inner slope (DMS04; Fukushige et al. 2004).

3.1 Results of run DM25

Run DM25 has an effective resolution corresponding to 127 million particles within the virial radius and a force resolution of $0.48 \times 10^{-3} r_{\rm vir}$. At this up to now unmatched resolution, the inner slope is roughly constant from the resolved radius (see Fig. 4) out to about one per cent of the virial radius of the final cluster.

Run D12 resolves the same cluster with 14 million particles and shows no convergence to a constant inner slope. Note that the 'D' cluster is one of six clusters analysed in DMS04 and its inner profile is not special and rather close to the sample average.

Fig. 4 indicates that there is a cusp in the centres of CDM clusters and it becomes apparent only at this very high numerical resolution.

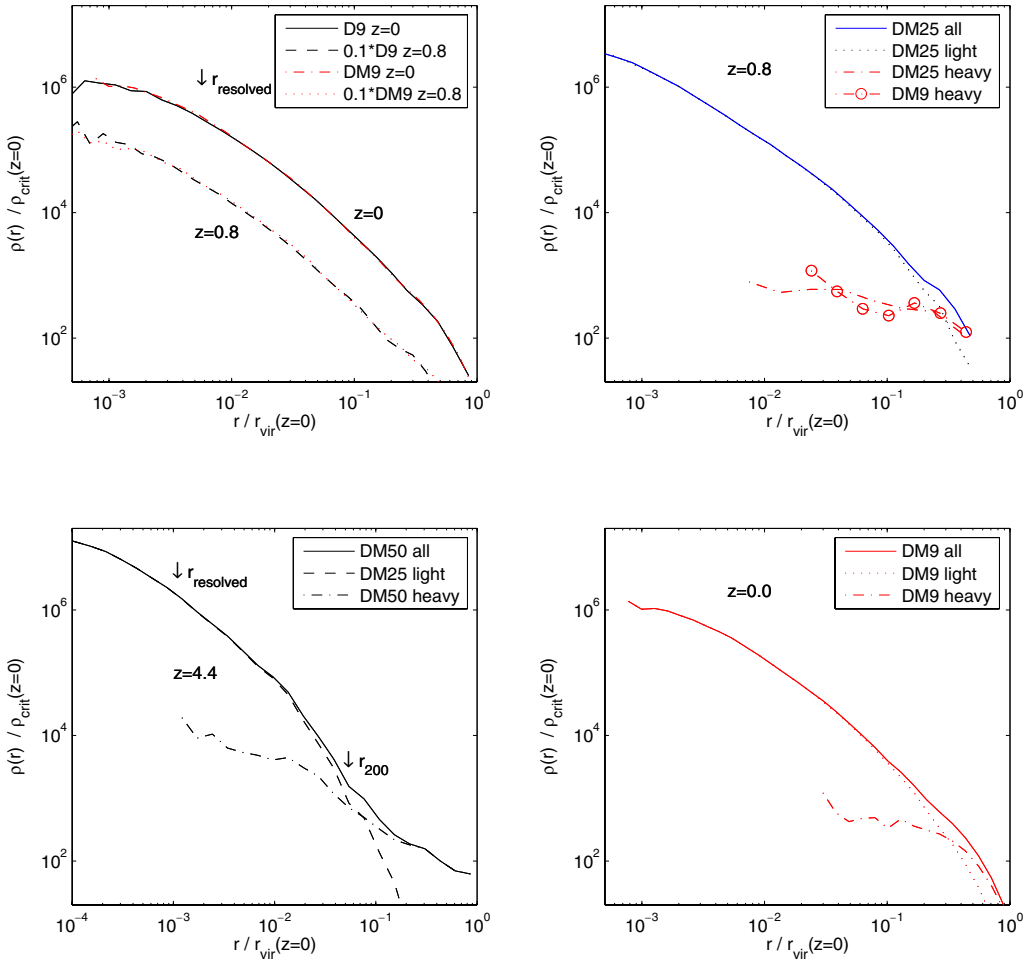

Figure 3. Tests of multimass refinement and convergence. The upper left-hand panel shows that run D9, which contains only high-resolution particles within the virial radius, has the same density profile as the multimass run DM9. The $z = 0.8$ profiles are shifted downward by a factor of 10 for clarity. The arrows indicate the convergence radius of run D9 estimated in DMS04. The lower left-hand panel shows the high- and low-resolution particles in run DM50 at $z = 4.4$. The panels on the right illustrate the mixing of light and heavy particles in runs DM9 and DM25 which have the same refinement regions.

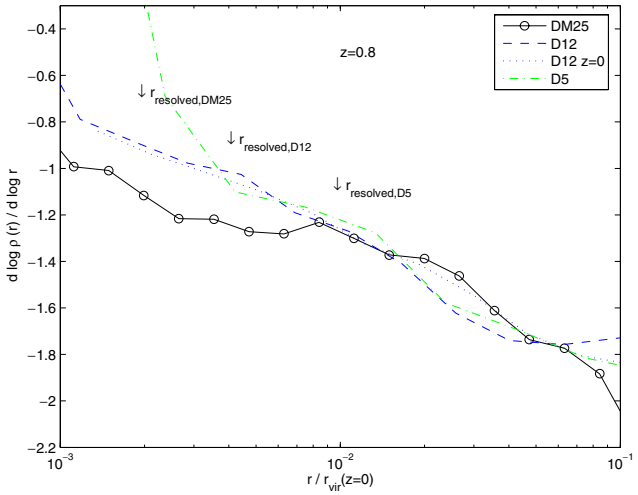

Figure 4. Logarithmic slope of the density profile of run DM25 at $z = 0.8$. The slopes of runs D5 and D12 at $z = 0.8$ and $z = 0$ are also shown for comparison. The arrows indicate the estimated convergence radii. Note that although the densities at the converged scales are within 10 per cent, the density gradients can already be substantially smaller.

The non-constant slopes just near the convergence scale are probably due to the first signs of numerical flattening that set in at this scale. At higher densities below the resolved scales one cannot make any robust predictions yet, but if one has to extrapolate into this region Fig. 4 motivates the choice of a cusp $\rho(r) \propto r^{-\gamma}$ with $\gamma \simeq 1.2$.

3.2 Resolving the very inner density profile at $z = 4.4$ (run DM50)

Mass accretion histories show that the inner part of CDM haloes is assembled in an early phase of fast accretion (van den Bosch 2002; Wechsler et al. 2002; Zhao et al. 2003) and recent high-resolution simulations have revealed that the inner density profile does not evolve at low redshift (Fukushige et al. 2004; Tasitsiomi et al. 2004; Reed et al. 2005). Fig. 4 confirms that the inner density profiles of runs D12 and D5 do not change from $z = 0.8$ to $z = 0$.

Therefore, in run DM50 we focus our computational effort even more on the early evolution of the inner profile. We refine the inner region of the most massive progenitor identified in run DM25 at $z = 4.4$. Because the refinement region needed is much smaller than that of DM9 or DM25 and we only run the simulation to $z = 4.4$, it is feasible to go to a much better mass and force resolution. The

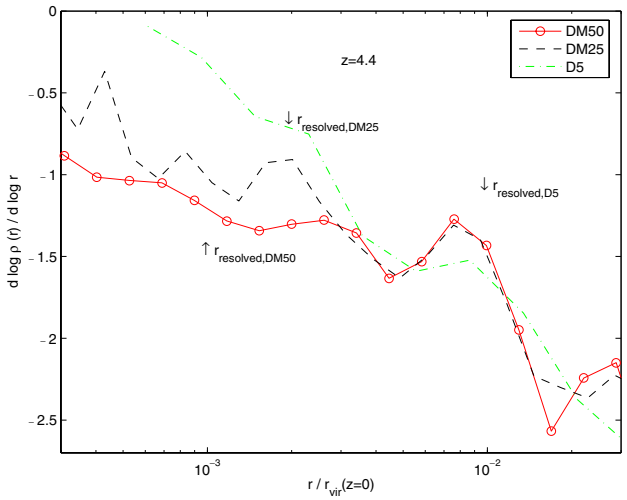

Figure 5. Logarithmic slope of the density profiles of runs D5, DM25 and DM50 at $z = 4.4$. The arrows indicate the estimated convergence radii. A constant inner slope of about -1.2 is evident in the highest-resolution run DM50. The increase of the slopes around the resolved radii is due to the onset of numerical flattening.

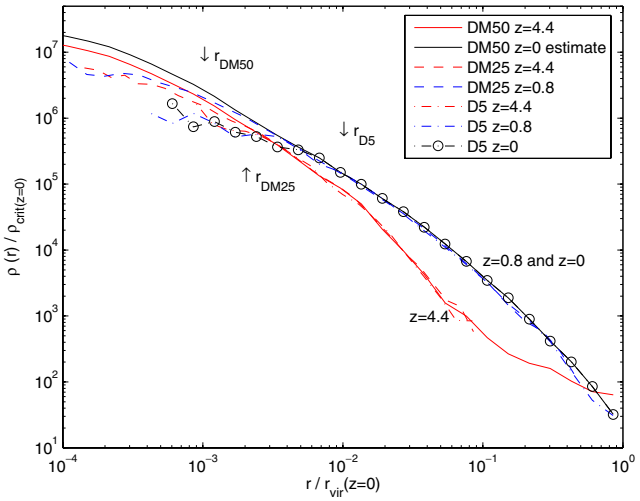

Figure 6. Density profiles in physical (not comoving) coordinates at redshifts 4.4, 0.8 and 0. Arrows mark the resolved scales of each run. The densities in the inner part do not evolve between $z = 0.8$ and $z = 0$ and the inner slopes remain constant even from $z = 4.4$ to $z = 0$. Using these observations we are able to estimate the final profile of a billion particle halo (upper solid line).

high-resolution particles in run DM50 are a billion times lighter than the final cluster.

Fig. 5 shows that the density profile of run DM50 at $z = 4.4$ is cuspy down to the resolved radius (0.1 per cent of the final virial radius). As in run DM25, the slopes begin to shallow just at the converged scale due to numerical flattening. The profile of DM50 at $z = 4.4$ supports the finding from run DM25 that the inner profile follows a steep power law $\rho \propto r^{-1.2}$. At the higher resolution of run DM50 we find substantially higher physical densities in the cluster centre at $z = 4.4$ compared to lower-resolution runs such as DM25. This suggests that a run such as DM50 evolved to low redshift would also yield substantially higher central densities as currently resolved in the centres of runs such as D12 and DM25.

3.2.1 Estimating the $z = 0$ profile of a billion particle halo

Now we go one step further and use the information from all the 'D'-series runs to try to estimate the density profile one would obtain if one simulates this cluster with a billion particles all the way to present time, a run which would be possible but extremely expensive with today's computational resources. From Fig. 6 we find that the density profile of run DM25 near its resolution scale shifts upward by a constant factor of 1.4 from $z = 4.4$ to $z = 0.8$. The density around $0.01\, r_{\mathrm{vir,z=0}}$ is constant from $z = 0.8$ to $z = 0$ (see run D5 in Fig. 6). The inner density profile slopes are constant even longer, i.e. from $z = 4.4$ to $z = 0$ (see Figs 4 and 5). Therefore, we estimate the $z = 0$ profile of run DM50 by rescaling the $z = 4.4$ profile of DM50 by a factor of 1.4 and using the $z = 0$ profile of run D12 outside $0.005 r_{\mathrm{vir,z=0}}$ (see Fig. 6). The extrapolated $z = 0$ profile of run DM50 should be regarded as a best guess for the density profile of an average CDM cluster resolved with a billion particles. A (multimass) simulation with this (effective) resolution evolved to redshift zero would be needed to check the accuracy of the estimate performed here. Note that our conclusions are based on the $z = 0.8$ results from run DM25 and not on the somewhat uncertain $z = 0$ extrapolation proposed in this section (but they are consistent with it).

3.3 Inner slope estimates based on the enclosed mass

For a mass distribution which follows $\rho(r) \propto r^{-\gamma}$ all the way in to $r = 0$ the slope γ can be calculated at any radius using the local density and the mean enclosed density (Navarro et al. 2004): $\gamma^*(r) = 3[1 - \rho(r)/\bar{\rho}(<r)]$. For simulated CDM density profiles, where γ becomes smaller towards the centre, $\gamma^*(r)$ is an upper limit for the asymptotic inner slope as long as both $\rho(r)$ and $\bar{\rho}(<r)$ have fully converged at radius r. Convergence tests show that the enclosed density $\bar{\rho}(<r)$ converges slower than the local density and $\bar{\rho}(<r)$ is generally underestimated near r_{resolved} due to missing mass within r_{resolved} (Power et al. 2003; DMS04). Fig. 7 shows $\gamma^*(r)$ for the two highest-resolution runs available at $z = 4.4$ and $z = 0.8$. We also plot the fractions of the local densities of the two runs and the fractions of enclosed densities to illustrate the different convergence scales of local and cumulative quantities. Fig. 7 confirms that at the estimated resolved scales for D12 and DM25 the local densities are within 10 per cent of the higher-resolution runs.[2] The typical differences are even smaller (about 5 per cent). The enclosed density $\bar{\rho}(<r)$ however converges slower: at r_{resolved} we find that the values are only about 0.83 of those measured in the higher-resolution runs. This causes the ratio $\rho(r_{\mathrm{resolved}})/\bar{\rho}(<r_{\mathrm{resolved}})$ to be underestimated (about 0.87 of the true value). This propagates into a larger relative error in $\gamma^*(r_{\mathrm{resolved}})$, which turns out to be too low by about 0.3 for the profiles studied here (given the arrows at r_{resolved} in Fig. 7). The different convergence rates of local and cumulative quantities tend to produce artificially low $\gamma^*(r)$ values and this effect becomes especially large near r_{resolved}. The significance of $\gamma^*(r)$ appears to be difficult to interpret, but the convergence tests presented here and in DMS04 suggest that $\gamma^*(r_{\mathrm{resolved}})$ is not a robust upper limit for the asymptotic inner slope.

[2] We determine r_{resolved} by demanding that the local density has to be within 10 per cent of the value from a much higher-resolution run and in cases where no such run is available the measured convergence radii from lower-resolution runs are rescaled using the mean interparticle separation $r_{\mathrm{resolved}} \propto N_{\mathrm{vir}}^{-1/3}$ (see DMS04).

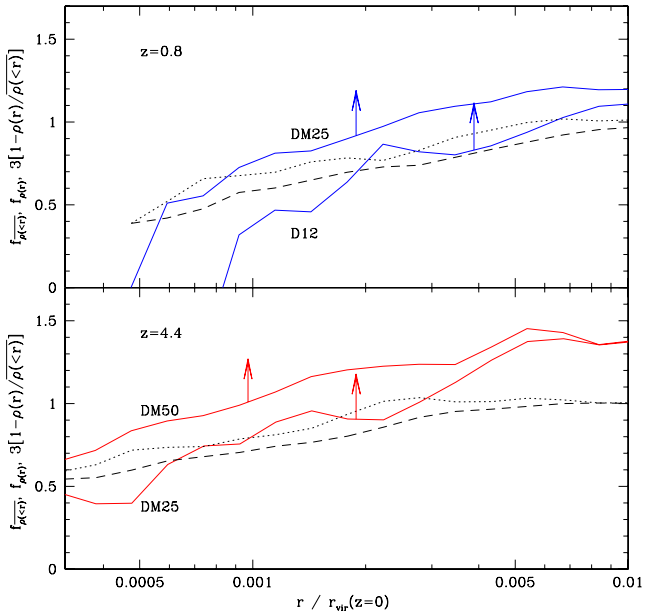

Figure 7. $\gamma^*(r)$ for the two highest-resolution runs at $z = 4.4$ and $z = 0.8$ (solid lines) and fractions of the densities of these two runs [dotted lines for $\rho(r)$ and dashed lines for $\bar{\rho}(<r)$]. Due to different convergence rates in local and cumulative quantities $\gamma^*(r)$ values from the lower-resolution runs lie below the higher-resolution results in the inner part of the halo. The arrows at $r_{\rm resolved}$ correct for this effect based on the following observations. The ratio $\rho(r_{\rm resolved})/\bar{\rho}(<r_{\rm resolved})$ is typically underestimated (0.87 of the high-resolution value) due to a small deficit in local density (0.95 of the true value) and a larger one in the enclosed density (0.83 of the true value) due to missing mass in the innermost regions. Underestimating $\rho(r_{\rm resolved})/\bar{\rho}(<r_{\rm resolved})$ by 0.87 leads to γ^* values which are too small by about 0.3.

3.4 Cored and cuspy fitting functions

In this section we fit one cuspy and two recently proposed cored functions to the density profiles of DM25 at $z = 0.8$ and to the tentative $z = 0$ extrapolation from run DM50. From the previous section we expect the cuspy function to work better in the inner part but we try to fit also the cored profiles for comparison.

We use a general $\alpha\beta\gamma$-profile that asymptotes to a central cusp $\rho(r) \propto r^{-\gamma}$:

$$\rho_{\rm G}(r) = \frac{\rho_{\rm s}}{(r/r_{\rm s})^{\gamma}\left[1 + (r/r_{\rm s})^{\alpha}\right]^{(\beta-\gamma)/\alpha}}. \quad (3)$$

If we take α, β and γ as free parameters, we encounter strong degeneracies, i.e. very different combinations of parameter values can fit a typical density profile equally well (Klypin et al. 2001). Therefore, we fix the outer slope $\beta = 3$ and the turnover parameter $\alpha = 1$. For comparison, the NFW profile has $(\alpha, \beta, \gamma) = (1, 3, 1)$, and the M99 profile has $(\alpha, \beta, \gamma) = (1.5, 3, 1.5)$. We fit the three parameters γ, $r_{\rm s}$ and $\rho_{\rm s}$ to the data.

Navarro et al. (2004) have proposed a different fitting function which curves smoothly over to a constant density at small radii:

$$\ln[\rho_{\rm N}(r)/\rho_{\rm s}] = (-2/\alpha_{\rm N})\left[(r/r_{\rm s})^{\alpha_{\rm N}} - 1\right]. \quad (4)$$

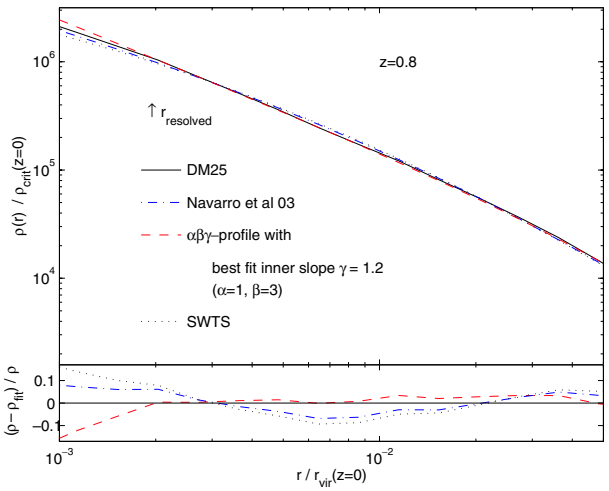

Figure 8. Density profile of run DM25 at $z = 0.8$ and fits with three different functions.

$\alpha_{\rm N}$ determines how fast this profile turns away from a power law in the inner part. Navarro et al. (2004) have found that $\alpha_{\rm N}$ is independent of halo mass and $\alpha_{\rm N} = 0.172 \pm 0.032$ for all their simulations, including galaxy and dwarf haloes.

Another profile that also curves away from power-law behaviour in the inner part was proposed by Stoehr et al. (2002):

$$\rho_{\rm SWTS}(r) = \frac{V_{\rm max}^2}{4\pi G} 10^{-2a_{\rm SWTS}[\log(r/r_{\rm max})]^2} \frac{1}{r^2} \times \left[1 - 4a \log\left(\frac{r}{r_{\rm max}}\right)\right]. \quad (5)$$

Here, $V_{\rm max}$ is the peak value of the circular velocity, $r_{\rm max}$ is the radius of the peak and $a_{\rm SWTS}$ determines how fast the profile turns away from a power law near the centre. Stoehr (2004) found that cluster profiles are well fitted with this formula using $a_{\rm SWTS}$ values between 0.093 and 0.15.

These three functions were fitted to the data from $z = 0.8$ by minimizing the relative density differences in each of about 20 logarithmically spaced bins in the range resolved by DM25 (i.e. from $0.0019 r_{\rm vir,z=0} = 3.3$ kpc to $r_{\rm vir,z=0} = 1750$ kpc). At $z = 0$, we use the resolved range of D12 for the fits (i.e. from $0.0039 r_{\rm vir,z=0} = 6.8$ kpc to $r_{\rm vir,z=0}$). The resulting best-fitting values and the root mean squares of the relative density differences are given in Table 2.

At $z = 0.8$, the average residuals of the three fits are similar, but they are dominated by the contribution from the outer parts of the cluster (see fig. 6 in DMS04). Figs 8 and 9 show that in the inner part the cuspy profile describes the data better. Both cored profiles underestimate the measured density at the resolution limit, both at $z = 0.8$ and in the estimated $z = 0$ profile. These profiles lie below the measured density profiles even inside $r_{\rm resolved}$ where one has to expect that the next generation of simulations will be able to resolve even higher densities.

Figs 10 and 11 show the slopes of the simulated profile in comparison with the slopes of the best fits. Again it is evident that

Table 2. Density profile parameters of run DM25 at $z = 0.8$ and of DM50 extrapolated to $z = 0$. Δ is the root mean square of $(\rho - \rho_{\rm fit})/\rho$ for the three fitting functions used.

Redshift	$\gamma_{\rm G}$	$r_{\rm sG}$ (kpc)	$\Delta_{\rm G}$	$\alpha_{\rm N}$	$r_{\rm s\,N}$ (kpc)	$\Delta_{\rm N}$	$a_{\rm SWTS}$	$r_{\rm max\,SWTS}$ (kpc)	$\Delta_{\rm SWTS}$
0.8	1.20	260	0.075	0.157	233	0.076	0.130	565	0.087
0.0	1.20	283	0.059	0.162	236	0.133	0.140	518	0.179

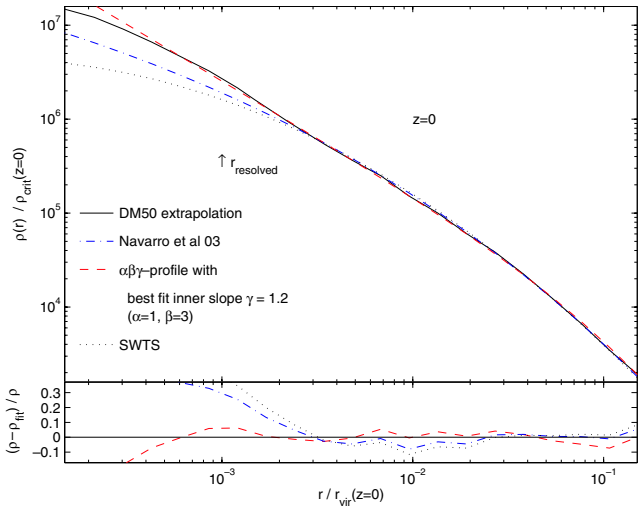

Figure 9. Density profile of run DM50 extrapolated to $z = 0.0$ and fits with three different functions.

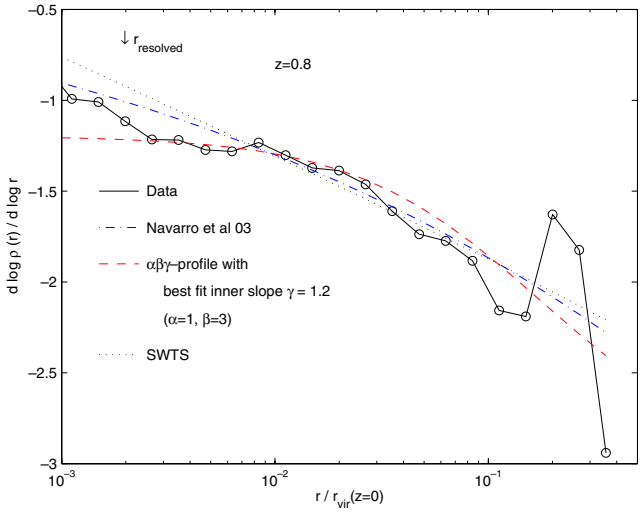

Figure 10. Logarithmic slopes of the measured and fitted density profiles from Fig. 8.

in the inner part the cuspy profile describes the real density run better.

4 CONCLUSIONS

The main conclusions of this work are the following.

(i) It is possible to use different mass particles to resolve one halo in cosmological CDM simulations without affecting the resulting density profiles.

(ii) This 'multimass' technique allows a reduction of the necessary number of particles and the computational cost by at least one order of magnitude without loss of resolution in the central region of the halo.

(iii) We confirm that the inner profile of a typical CDM cluster does not evolve since about redshift one.

(iv) The logarithmic slope of the dark matter density profile converges to a roughly constant value in the inner part of cluster haloes. This probably holds also for smaller systems (such as galaxy and

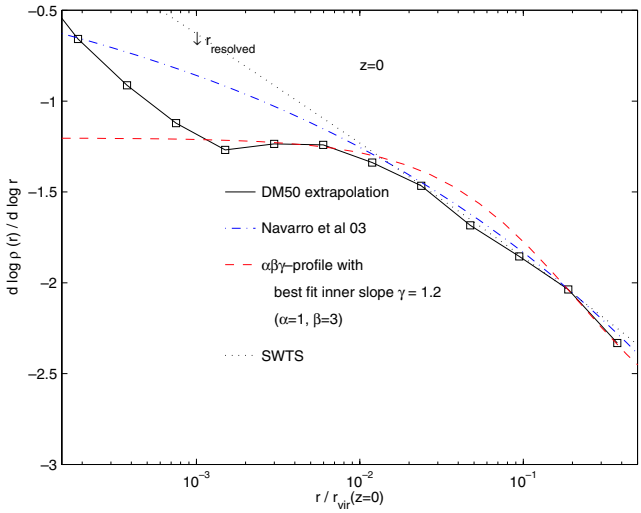

Figure 11. Logarithmic slope of the extrapolated $z = 0$ DM50 density profile and of the fitted density profiles from Fig. 9.

dwarf haloes) but there it is even more difficult to numerically resolve the cusps.

(v) At resolutions around 10 million particles per halo, the inner slope appears to approach zero continuously but this impression is caused by numerical flattening of the profiles due to insufficient mass resolution.

(vi) The cluster studied here has a central cusp $\rho \propto r^{-\gamma}$ with a slope of about $\gamma = 1.2$. From earlier studies (DMS04) we expect this inner profile to be close to the average and the scatter is about 0.15.

(vii) Profiles with a core (Stoehr et al. 2002; Navarro et al. 2004) underestimate the measured dark matter density at (and even inside) the current resolution limit.

ACKNOWLEDGMENTS

We would like to thank Piero Madau and Mike Kuhlen for useful discussions, and the referee for valuable suggestions. All computations were performed on the zBox supercomputer at the University of Zurich. JD is supported by the Swiss National Science Foundation.

REFERENCES

Ahn K. J., Shapiro P. R., 2005, MNRAS, 363, 1092
Bertone G., Merrit D., 2005, Mod. Phys. Lett. A, 20, 1021
Bertschinger E., 2001, ApJSS, 137, 1
Binney J., 2004, MNRAS, 350, 939
Binney J., Knebe A., 2002, MNRAS, 333, 378
Calcáneo-Roldán C., Moore B., 2000, Phys. Rev. D, 62, 123005
Colin P., Avila-Reese V., Valenzuela O., 2000, ApJ, 542, 622
Colín P., Klypin A., Valenzuela O., Gottlöber S., 2004, ApJ, 612, 50
Dawson J. M., 1983, Rev. Mod. Phys., 55, 403
deBlock W. J., McGaugh S. S., Bosma A., Rubin V. C., 2001, ApJ, 552, L23
Diemand J., Moore B., Stadel J., Kazantzidis S., 2004a, MNRAS, 348, 977
Diemand J., Moore B., Stadel J., 2004b, MNRAS, 353, 624 (DMS04)
Diemand J., Moore B., Stadel J., 2005, Nat, 433, 389
Flores R. A., Primack J. R., 1994, ApJ, 427, L1
Fukushige T., Makino J., 1997, ApJ, 477, L9
Fukushige T., Makino J., 2003, ApJ, 588, 674

Fukushige T., Kawai A., Makino J., 2004, ApJ, 606, 625
Gao L., White S. D. M., Jenkins A., Frenk C., Springel V., 2005, MNRAS, 363, 379
Ghigna S., Moore B., Governato F., Lake G., Quinn T., Stadel J., 2000, ApJ, 544, 616
Hansen S. H., Moore B., 2005, MNRAS, submitted (astro-ph/0411473)
Klypin A., Kravtsov A. V., Bullock J. S., Primack J. R., 2001, ApJ, 554, 903
Kuhlen M., Strigari L. E., Zentner A. R., Bullock J. S., Primack J. R., 2005, MNRAS, 357, 387
Macciò A. V., Quercellini C., Mainini R., Amendola L., Bonometto S. A., 2004, Phys. Rev. D, 69, 123516
Moore B., 1994, Nat, 370, 629
Moore B., Governato F., Quinn T., Stadel J., Lake G., 1998, ApJ, 499, L5
Moore B., Quinn T., Governato F., Stadel J., Lake G., 1999, MNRAS, 310, 1147
Moore B., Calcáneo-Roldán C., Stadel J., Quinn T., Lake G., Ghigna S., Governato F., 2001, Phys. Rev. D, 64, 063508
Moore B., Diemand J., Stadel J., 2004, in Diaferio A., ed., Proc. IAU Colloq. 195, Outskirts of Galaxy Clusters: Intense Life in the Suburbs. Kluwer, Dordrecht, p. 513
Navarro J. F., Frenk C. S., White S. D. M., 1996, ApJ, 462, 563
Navarro J. F. et al., 2004, MNRAS, 349, 1039
Power C., Navarro J. F., Jenkins A., Frenk C. S., White S. D. M., Springel V., Stadel J., Quinn T., 2003, MNRAS, 338, 14
Prada F., Klypin A., Flix J., Martinez M., Simonneau E., 2004, Phys. Rev. Lett., 93, 241, 301
Reed D., Governato F., Verde L., Gardner J., Quinn T., Stadel J., Merritt D., Lake G., 2005, MNRAS, 357, 82
Salucci P., Burkert A., 2000, ApJ, 537, L9
Simon J. D., Bolatto A. D., Leroy A., Blitz L., Gates E. L., 2005, ApJ, 621, 757
Springel V., White S. D. M., Tormen G., Kauffmann G., 2001, MNRAS, 328, 726
Stadel J., 2001, PhD thesis, Univ. of Washington
Stoehr F., 2005, MNRAS, in press (doi:10.1111/j.1365-2966.2005.09676.x)
Stoehr F., White S. D. M., Tormen G., Springel V., 2002, MNRAS, 335, L84
Swaters R. A., Madore B. F., van den Bosch F. C., Balcells M., 2003, ApJ, 583, 732
Tasitsiomi A., Kravtsov A. V., Gottlober S., Klypin A. A., 2004, ApJ, 607, 125
van den Bosch F. C., 2002, MNRAS, 331, 98
van den Bosch F. C., Swaters R. A., 2001, MNRAS, 325, 1017
Wechsler R. H., Bullock J. S., Primack J. R., Kravtsov A. V., Dekel A., 2002, ApJ, 568, 52
Zhao D., Mo H., Jing Y., Börner G., 2003, MNRAS 339, 12

This paper has been typeset from a TEX/LATEX file prepared by the author.